



## Plasma Spraying and Characterization of Chromium Carbide-Nickel Chromium Coatings

P. Ctibor<sup>1</sup>, M. Prantnerová<sup>2</sup>

<sup>1</sup> Materials Engineering Department, Institute of Plasma Physics ASCR, Za Slovankou 3, 182 00, Praha 8, Czech Republic.

<sup>2</sup> Thermal Spray Division, Research and Testing Institute Pilsen, Tylova 57, 316 00, Plzeň, Czech Republic.

### ARTICLE INFO

#### Article history:

Received: 16 Mar 2016

Final Revised: 27 Sept 2016

Accepted: 24 Oct 2016

Available online: 25 Oct 2016

#### Keywords:

Plasma spraying

Chromium carbide

Slurry abrasion

Dry rubber wheel test

Friction

Microhardness

### ABSTRACT

Chromium carbide – nickel chromium powder ( $Cr_3C_2$ -25wt%NiCr) was plasma sprayed by a water-stabilized system WSP<sup>®</sup>. A series of experiments with variable feeding distance was carried out. Basic characterization of coatings was done by XRD, SEM and light microscopy plus image analysis. Microhardness was measured on polished cross sections. The main focus of investigation was on resistances against wear in dry as well as wet conditions. The appropriate tests were performed with set-ups based on ASTM G65 and G75, respectively. The influence of spray parameters on coating wear performance was observed. The results of mechanical tests are discussed in connection with changes in the character of the coating's microstructure. The results show that for obtaining the best possible  $Cr_3C_2$ -25NiCr coating with WSP<sup>®</sup> process, from the wear resistance point of view, medium feeding distance is desired and its decrease or increase leads to certain worsening of studied properties. Prog. Color Colorants Coat. 9 (2016), 281-290 © Institute for Color Science and Technology.

### 1. Introduction

Cermets are ceramic–metal composites that are made of ceramic phase and metal binder phase. Cermets are designed to have the optimal properties of both ceramics, such as high temperature stability and hardness, and those metals, such as the ability to undergo plastic deformation [1]. Combination of such important properties as high hardness, good strength, medium fracture toughness and excellent oxidation resistance results in growing interest to  $Cr_3C_2$  based cermets. Primarily covalent bonding exhibited by carbides provides many of the key properties required for advanced applications, including high stiffness and

high specific strength at elevated temperatures. However, covalent bonding makes these compounds brittle at ambient temperature. As a result these materials have a low damage tolerance. Despite of the limitations, refractory chromium carbide based composites have a wide use in industry. Structural applications include bearings, seals, valve seats and orifices. The method of fabrication may influence the properties and therefore reliability of cermets to a great extent. Wear resistance of composites is not strictly a material property, but mostly depends on microstructural features that determine the materials response to the specific stress state imposed by

\*Corresponding author: ctibor@ipp.cas.cz

aggressive media.

$\text{Cr}_3\text{C}_2$  based cermets with Ni or NiCr as metal matrix are typically sprayed with High Velocity Oxy-Fuel (HVOF) technique [2]. They exhibit less excellent wear resistance than WC-based cermets [3] but are very stable at elevated temperatures [4] and their wear resistance is definitively better than that of all ceramics and metals [3].

Atmospheric/ambient Plasma Spraying (APS) with gas-stabilized conventional torch (GSP) was used to spray 10 mm thick  $\text{Cr}_3\text{C}_2$ -NiCr coatings [4]. Friction coefficient of 0.8, higher than that of WC-Co, was measured for HVOF coatings [2] whereas similar values were reported for APS coatings and lower values for coatings plasma sprayed in a controlled atmosphere, where graphite carbon was detected by XRD as a product of carbide decomposition [5]. Several attempts to enhance the cermet coatings performance were employed including preparation of nano-structure based coatings [6], use of a detonation gun spraying [7], shrouded plasma spray [8] or even replacement of carbide component by a less sensitive material, e.g.  $\text{TiB}_2$  [9]. Recent advances in the processing technology enable performing post-treatment of sprayed coatings with spark plasma sintering, which was demonstrated to close cracks in plasma sprayed  $\text{Cr}_3\text{C}_2$ -NiCr [10].

It was revealed that carbon loss and  $\text{Cr}_3\text{C}_2$  loss during flight of particles at HVOF spraying were very limited [11]. The rebounding of large carbide particles on impact [12] was the dominant factor to result in carbon loss and carbide loss. A carbon loss during coating deposition is also typical for plasma spray process because of its extremely high temperature. The largest part of carbon loss takes place after the spray particles impact on the substrate surface, whereas the loss during particles in-flight is rather limited [13].

Extensive carbide dissolution in the NiCr matrix generates widespread grayscale variation in SEM-BE micrographs, indicative of marked variation in the matrix composition. The retained carbide grains were predominately in the center of the larger lamellae [4]. The coating consists of a metallic Ni-Cr matrix having different shades of gray, rich in Cr and C from the  $\text{Cr}_3\text{C}_2$  phase dissolved in the Ni-Cr matrix to a different extent, together with mixed carbide interspersed with voids [13]. An average porosity value of  $4.3 \pm 0.2\%$  was determined for the coating by image analysis [13]. The presence of oxides contributed to coating inhomogeneity and an appreciable decrease in cohesion [5] reflected in wear surface character.

This paper aims to examine the applicability of a high feed-rate WSP<sup>®</sup> spray setup [14], that is able to process up to tens of kilograms of metal or cermet material per hour for spraying of  $\text{Cr}_3\text{C}_2$ -25wt% NiCr material and evaluate the resulting coatings from the relevant viewpoints. All spray runs were carried out in the ambient atmosphere, as is usual in this process called atmospheric plasma spraying (APS).

## 2. Experimental procedure

### 2.1. Powder and spraying

The powder  $\text{Cr}_3\text{C}_2$ -25wt% NiCr (NiCr having composition 80% Ni-20% Cr) was a commercial product labeled PT-3003SC-39 (Plasmatec, Montreal, Canada). The nominal size of this powder was 100 to 140  $\mu\text{m}$ . The powder was produced via sintering with subsequent crushing, which produces the non-convex surface and also elongated shape. According to histogram on Figure 1, certain amount of the particles larger than 200  $\mu\text{m}$  is present and also several percent of fine particles finer than 50  $\mu\text{m}$  are present.

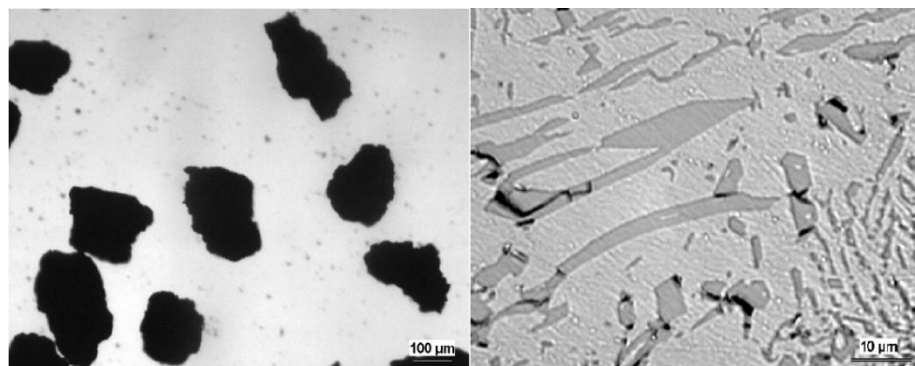


**Figure 1:** Shape and size of the feedstock powder (left) and detail of the cut and polished particle (right); light microscopy.

Spraying was carried out by a water-stabilized plasma gun WSP<sup>®</sup> 500. Feeding distance, FD, varied – 70, 85 and 100 mm, whereas spray distance, SD, was fixed at 350 mm. Arc power of 153.6 kW (given by approx. 480 A and 320 V); feed rate of 15 kg/h (i.e. 250 g/min) and powder injection angle of 60° were used as a setup parameters. Powder was fed into the plasma jet by two injectors and forced in by Ar gas with flow rate of 3.2 slpm. Substrates were preheated to 180°C in all cases. Coatings with thickness about 1 mm were developed on stainless steel and carbon steel substrates. The cooling speed is rather low for thick Cr<sub>3</sub>C<sub>2</sub>-NiCr coating on low-conductivity stainless steel. All substrates were grit blasted before spraying by alumina grit (0.6 mm) and the final roughness of R<sub>a</sub> about 10 µm. The maximum temperature measured during spraying was 400 °C.

### 2.2. Characterization techniques

Powder size distribution was determined by the laser scattering device Analysette 22 (Fritsch, Germany) in H<sub>2</sub>O+Na<sub>4</sub>P<sub>2</sub>O<sub>7</sub>. Scanning electron microscope Camscan 4DV (Camscan, UK), and light microscope Neophot 32 equipped by a CCD camera were used for structural investigation. X-rays diffractometer D 500 (Siemens AG, Germany) with filtered Cu radiation was used for phase analysis. Angle 2theta from 10 to 90° was recorded with step 0.02°.

Porosity was studied by the light microscopy on polished cross sections. Micrographs were taken with a CCD camera and processed using the image analysis (IA) software (Lucia G, Laboratory Imaging, Prague, Czech Republic). A series of 10 images of microstructures taken from various areas of a cross section for each sample were analyzed. The magnification allowed an analysis of all objects with size of 3 microns or more for pores as well as oxides content quantification. After proper threshold setting of the gray levels the porosity is black, the metallic material is light and the oxides are darker (dark gray) in optical micrographs. The reason is that reflection from metals is stronger than oxides. For calculation of the oxide content the same images as for porosity.

Microhardness was measured by the Hanemann microhardness head mounted on the light microscope with fixed load of 1 N and the Vickers indenter on a microhardness head (Carl Zeiss, Germany) attached to the light microscope Neophot 2. Twenty indentations from various areas of a cross section for each sample

were analyzed.

Slurry abrasion response of coatings (SAR test) was measured according to a modified ASTM G-75 test [15]. The main modification contains the fact that ASTM emphasizes the use of a reference sample, which is a bulk alloy – targeted to compare with bulk metals and not with cermet coatings. Our modified version of the SAR test was used previously for variety of coatings [16-18]. The applied force is 22.24 N per specimen and alumina particles mixed with water serve as the abrasive slurry. The test involves a 9216 meters path divided into four increments. The mass loss was measured at the end of each 2304 m increment. Then the specimens were ultrasonically cleaned and weighed. Accuracy of the measurement was about ± 5 %.

Dry rubber wheel (traditionally called Dry Sand - Rubber Wheel; DSRW) abrasion test, a modified version of ASTM G-65 [19], was performed using alumina particles as abrasive. The modifications of the ASTM prescriptions were namely in the abrasive particle size and rubber type (hardness). The abrasive was fed between the coated sample and the rotating rubber wheel. The abrasive particle size was 250 to 450 µm. The samples were pressed against the rubber wheel with the force of 22 N. The test comprises 2000 revolutions of the wheel, which corresponds to a wear length of 1436 m. All the coating weight losses were converted to volume losses by applying densities measured by the Archimedean method, roughly 5.93 g/cm<sup>3</sup>. Accuracy of the measurement was approx. ± 8 %.

## 3. Results and discussion

### 3.1. Microstructure of the feedstock plasma sprayed coatings

Size and shape of the Cr<sub>3</sub>C<sub>2</sub>-NiCr powder used as feedstock for spray experiments are displayed in Figure 2. The surface of particles is not very smooth and some of them are elongated. Inside the particles the carbide itself is distributed randomly inside the matrix. Carbide grains (darker areas in the right image) are elongated with some pores (black) in them or just besides them. This fine porosity stems from powder production. The size distribution of Cr<sub>3</sub>C<sub>2</sub>-NiCr powder is displayed in Figure 3. Microstructure of sprayed coatings is also displayed in Figure 3 and the SEM-BE image of the coating FD 85 is shown in Figure 4. In

Figure 3, the higher is the FD, the larger are individual splats and also pores between them. Black color in Figure 4 corresponds to pores and the lightest gray ones show NiCr binder (dot 8). There is variety of gray levels between the maximum and minimum. It

indicates that the decomposition of  $\text{Cr}_3\text{C}_2$  in plasma reached various levels [8] also corresponding dot analysis indicates variation in Cr to Ni ratio. Among different gray levels one is characteristic for  $\text{Cr}_2\text{O}_3$  (dots 12, 15 and 16).

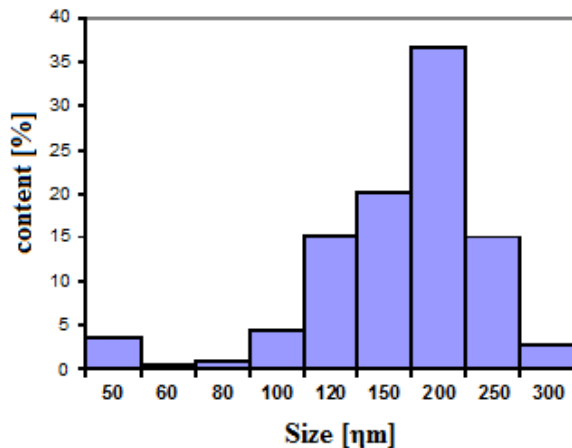


Figure 2: Size distribution of the  $\text{Cr}_3\text{C}_2$ -NiCr feedstock powder.

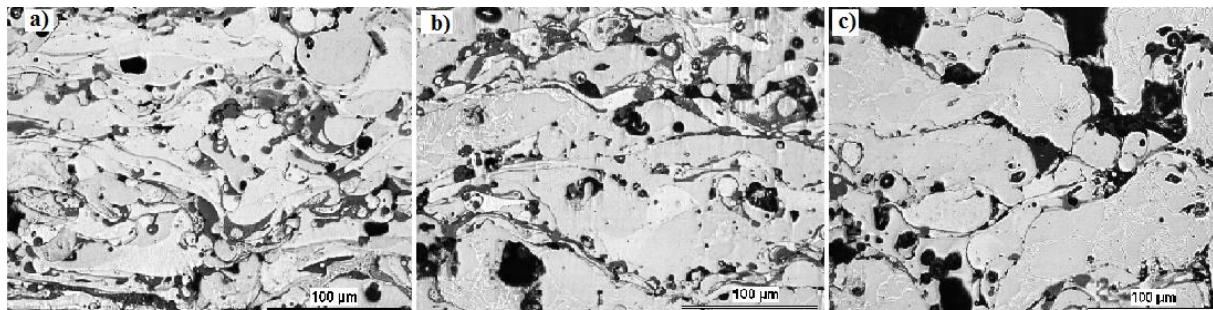


Figure 3: Microstructure of  $\text{Cr}_3\text{C}_2$ -NiCr coating cross section a) FD 70; b) 85; c) 100 mm; light microscopy.

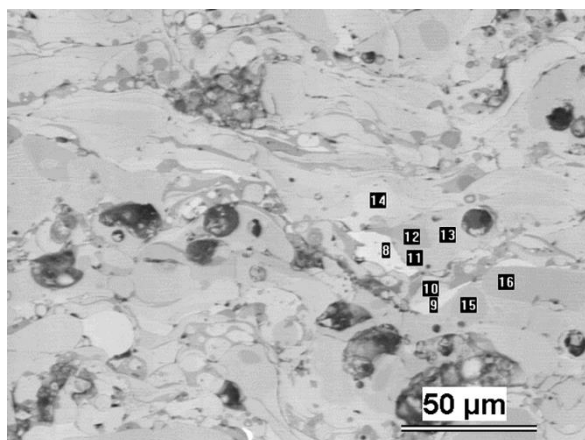


Figure 4: Microstructure of  $\text{Cr}_3\text{C}_2$ -NiCr coating cross section; SEM-BE; numbers correspond to Table 1.

The amount of various gray levels and weak difference between them makes detailed quantification of phase content from images nearly impossible. Cr and Ni molar percentage in various dots from Figure 4 is summarized in Table 1. Nickel presence at the dots, mentioned above as corresponding to Cr<sub>2</sub>O<sub>3</sub>, is closely to zero. Measurement of porosity and oxides was done on optical micrographs. Table 2 brings porosity P and oxide content OX obtained as area fraction by image analysis for coatings sprayed with SD 350 mm. It was observed that porosity P increases whereas oxide content OX decreases with increasing the FD. It means that increasing the feeding distance leads to more porous but less oxidized coatings. The porosity of FD 70 is low because of the fast movement of the particles at impact. In FD100, the particles travel larger distance (i.e. 30 mm) in plasma that is slowing down because of mixing with the surrounding ambient atmosphere. Because of this mixing, more oxidative atmosphere is present at FD100. The FD100 coating contains therefore more Cr<sub>2</sub>O<sub>3</sub>. The porosity is slightly higher than that of vacuum plasma sprayed coatings [9] which was reported as 4.3±0.2 %.

### 3.2. Phase composition

Figure 5 presents diffraction patterns of feedstock powder and coatings. XRD of the feedstock revealed the presence of Cr<sub>3</sub>C<sub>2</sub> (PDF 01-071-2287) as main phase with NiCr as a minor phase. In the FD100coating, Cr<sub>2</sub>O<sub>3</sub> (PDF 01-082-1484) was found as the only oxide phase. FD100coating retains NiCr from the feedstock whereas the coating from shorter FD not.

On the other hand, chromium oxide and carbon are also predominant in FD100 coating. We could presume that in this coating, oxidation and partial dissolution are the main phase changes whereas in shorter FD coatings which have longer dwell time in plasma, the origin of complicated mixed carbides (with peaks overlapped with the indicated Cr<sub>3</sub>C<sub>2</sub> peaks [2, 4]) is the main change. All coating patterns moreover contain a hump centered at 44°, which is a sign of partial amorphization. This amorphous fraction is typically attributed to Ni [20]. Cr<sub>2</sub>O<sub>3</sub> phase was found also in coatings sprayed in vacuum plasma spraying (in a protective chamber with the pressure reduced to 60 mbar) [13]. This indicates very high sensitivity of Cr<sub>3</sub>C<sub>2</sub>-NiCr to oxidation.

### 3.3. Properties of the coatings

The results of wear tests are summarized in Table 3. Wear coefficient is expressed in the same units for dry and wet test for easier comparison, however, the very different arrangement of both tests enables only very rough comparison. The lower the wear coefficient, the better is the wear resistance. We can observe that Cr<sub>3</sub>C<sub>2</sub>-NiCr coating sprayed using medium FD 85 mm at fixed SD 350 mm is more wear resistant than coatings sprayed with short FD 70 mm as well as long FD 100 mm. This trend is the same for wet (SAR) as well as dry (DSRW) conditions. The FD70 coating has the lowest porosity but the highest oxide content whereas the FD100 coating has the highest porosity and the lowest oxide content. The intermediate FD85 brings a compromise between porosity and oxidation, Table 2.

**Table 1:** Molar fraction [%] of Cr and Ni elements at dots indicated in Figure 3.

Dot No.	8	9	10	11	12	13	14	15	16
Cr	28	34	81	72	99	73	54	99	99
Ni	72	66	19	28	1	27	46	1	1

**Table 2:** Porosity P and oxide content OX in Cr<sub>3</sub>C<sub>2</sub>-NiCr coatings, including the annealed one (ann) at CTE measurement.

Coating	P [%]	OX [%]
FD70	6.8 ± 3.1	18.1 ± 1.6
FD85	11.6 ± 2.4	15.7 ± 2.7
FD100	13.4 ± 3.4	12.2 ± 1.9
FD70ann	2.3 ± 0.7	16.3 ± 3.5

**Table 3:** Wear and microhardness of Cr<sub>3</sub>C<sub>2</sub>-NiCr coatings in comparison with selected materials measured by the same techniques.

Sample	SAR - wear coef. [mm <sup>3</sup> /Nm]	DSRW - wear coef. [mm <sup>3</sup> /Nm]	HV <sub>0.1</sub> [GPa]
FD70	0.00035	0.00062	13.12 ± 4.60
FD70ann	0.00035	0.00062	17.57 ± 4.68
FD85	0.00019	0.00051	15.51 ± 4.34
FD100	0.00023	0.00059	14.24 ± 5.23
Cr <sub>3</sub> C <sub>2</sub> -NiCr, HVOF	0.00004	0.0004 [21]	7.86 ± 1.23
Hard chromium	0.00019	0.00056	8.84 ± 0.97
Low carbon steel (substrate)	0.00093	0.0018 [21]	6.02 ± 2.13

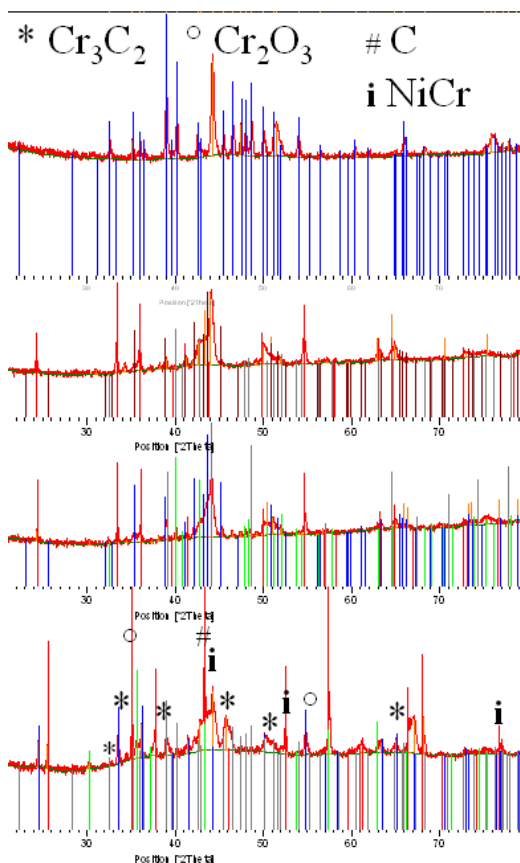


**Figure 5:** XRD patterns of Cr<sub>3</sub>C<sub>2</sub>-NiCr, from the top: feedstock powder; coatings FD 70; 85; 100 mm.

The powder melt is supposed to be warmer and faster at the moment of impact onto substrate when the FD decreases. This induces lower porosity and better cohesion. However, too short FD can lead to evaporation of fine powder particles and very rapid cooling (which can generate high residual stress), hence the coating quality diminishes. Shorter dwell time in plasma for feedstock fed at longer FD limits oxidation but supports porosity creation.

We can also conclude that the coarser powder (DSRW test) leads to dramatically higher wear. The wear is 3 to 6 times larger than with the fine powder. In fact, the larger particles of the wear medium are able to interact with the whole individual splats. This contributes markedly to wear loss of the coating in the case of the DSRW test.

All plasma sprayed coatings, especially the best one, exhibit comparable wear characteristics similar to

hard chromium, Table 3, and simultaneously higher microhardness. HVOF coating of  $\text{Cr}_3\text{C}_2\text{-NiCr}$  has even lower wear coefficient, which is due to the different microstructure of HVOF coating [2, 6, 11].

Microhardness of HVOF coating of  $\text{Cr}_3\text{C}_2\text{-25wt\% NiCr}$  with similar phase composition including mixed carbides was reported to be about 8 GPa [22, 23]. Spraying of  $\text{Cr}_3\text{C}_2\text{-NiCr}$  by a supersonic plasma gun [24] led to the presence of mixed carbides in the coating and strong indentation size effect on microhardness values that varied from 9.54 GPa at 20 mN to 6.37 GPa at 500 mN. When cold spray process was employed [25], the microhardness of  $\text{Cr}_3\text{C}_2\text{-25wt\% NiCr}$  coating was 8.43 GPa at 300 mN load. Also the crystallinity of the NiCr phase is decreased in the cold spray coating compare to the feedstock powder [25]. In some papers, higher load at DSRW is used [23, 26] (e.g. up to 130 N). Also in this case, the character of material removal exhibit a polished appearance without any macro-scale plastic deformation or chippings [23, 26]. High microhardness of our plasma sprayed coatings is accompanied by their high brittleness that is a cause of worse wear resistance compared to HVOF coatings. The role of ceramic phase, i.e.  $\text{Cr}_2\text{O}_3$ , is also of this character – brittle and hard component. As visible in the Figure 6, the carbides (dark areas in SEM-BE image) are homogeneously distributed and separated by relatively thin shells form from the binder phase (light areas in SEM-BE image).

The high hardness of the plasma sprayed coatings is because of the  $\text{Cr}_2\text{O}_3$  content. This oxide (not exists in HVOF coatings) is harder than  $\text{Cr}_3\text{C}_2$ . For the same reason the wear coefficient is higher than for HVOF. It means that plasma sprayed coatings are less wear resistant. The reason is the brittleness of  $\text{Cr}_2\text{O}_3$ . This brittle oxide contributes to cracking and local delamination of the plasma coatings at the wear tests. This increases the weight loss and so the wear coefficient. HVOF coatings are more ductile. Plasma coatings are hard but brittle. For the in-service behavior is it finally disadvantageous.

Thermal expansion coefficient (CTE) of the sample FD70 was measured by the vertical dilatometer Setsys 16/18 (Setaram, France) in Ar up to 1200 °C with heating and cooling ramps of 2 °C/min. The resulting thermal expansion coefficient is 9.0  $\mu\text{m/m.K}$ , which is comparable with other data reported for  $\text{Cr}_3\text{C}_2\text{-NiCr}$  coatings: 10.3  $\mu\text{m/m.K}$  [27] as well as with values relevant for pure  $\text{Cr}_3\text{C}_2$ : 10.3 to 10.4  $\mu\text{m/m.K}$  [28].

The sample was after the dilatometric test of CTE, which represents annealing in Ar atmosphere, sectioned and polished for measurements of porosity and oxide content (by image analysis) as well as microhardness (both with experimental approaches described above). Porosity reduced to  $2.3 \pm 0.7 \%$ , but oxides content only to  $16.3 \pm 3.5 \%$ , was detected by image analysis. The entire inhomogeneity of the coating was however preserved, Figure 7.

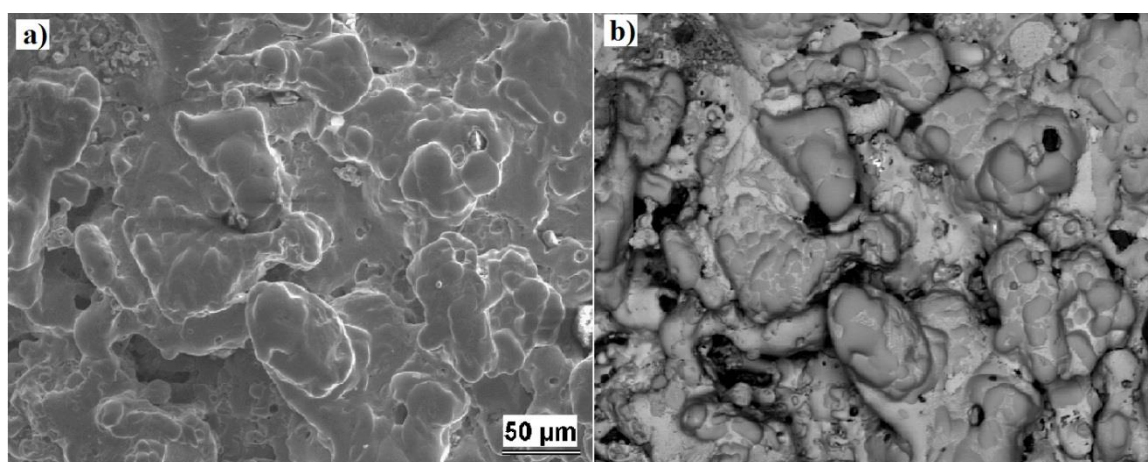


Figure 6: Surface of as-sprayed  $\text{Cr}_3\text{C}_2\text{-NiCr}$  coating: a)SEM-SE and b) SEM-BE from the same area.

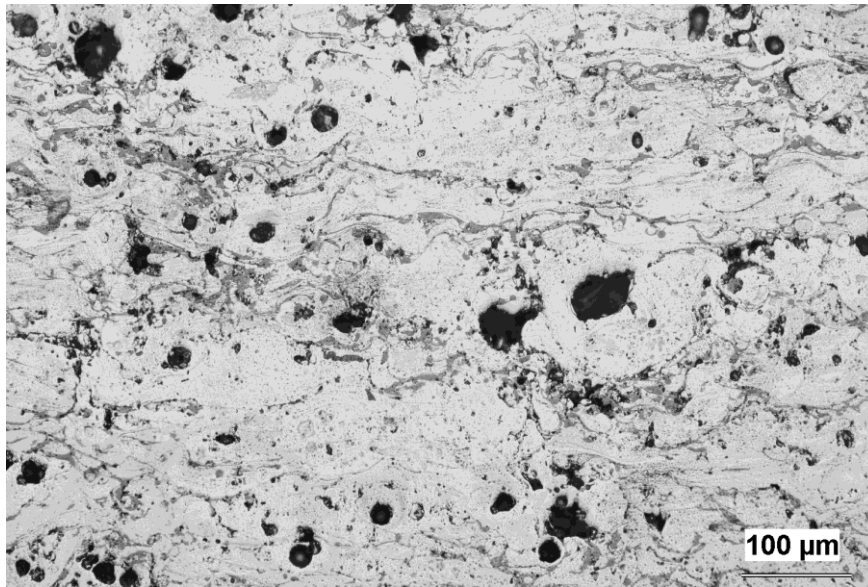


Figure 7: Microstructure of  $\text{Cr}_3\text{C}_2$ -NiCr coating annealed in dilatometric test; cross section, light microscopy.

#### 4. Conclusions

Chromium carbide – nickel chromium powder ( $\text{Cr}_3\text{C}_2$ -25wt% NiCr) was plasma sprayed by a high feed-rate water-stabilized system WSP<sup>®</sup> using a series of experiments with variable feeding distances FD. The results show that for obtaining the best possible  $\text{Cr}_3\text{C}_2$ -25wt% NiCr coating from wear resistance point of view, medium feeding distance is desired because the intermediate FD 85 mm brings the best compromise

between porosity and oxidation. All plasma sprayed coatings, especially the best one, exhibited comparable wear characteristics similar to hard chromium and simultaneously higher microhardness.

#### Acknowledgment

The authors acknowledge the help of B. Kolman (IPP Prague) with the electron microscopy and chemical elements analysis.

#### 5. References

1. I. Hussainova, J. Pirso, M. Antonov, K. Juhani, S. Letunovits, Erosion and abrasion of chromium carbide based cermets produced by different methods, *Wear*, 263(2007) 905-912.
2. W. Zorawski, S. Skrzypek, J. Trpcevska, Tribological Properties of Hypersonically Sprayed Carbide Coatings, *FME Transactions*, 36(2008), 81-88.
3. H. I. McClark, H. M. Hawthorne, Y. Xie, Wear rates and specific energies of some ceramic, cermet and metallic coatings determined in the Coriolis erosion tester, *Wear*, 233(1999), 319-328.
4. J. F. Li, L. Li, and C. X. Ding, Thermal diffusivity of plasma-sprayed  $\text{Cr}_3\text{C}_2$ -NiCr coatings, *Mat. Sci. Eng. A*, 394(2005), 229-240.
5. M. H. Staia, T. Valente, C. Bartuli, D. B. Lewis, C.

- P. Constable, A. Roman, J. Lesage, D. Chicot, G. Mesmacque, Part II: tribological performance of Cr<sub>3</sub>C<sub>2</sub>-25% NiCr reactive plasma sprayed coatings deposited at different pressures, *Surf. Coat. Technol.*, 146–147(2001), 563–570.
6. L. Fedrizzi, S. Rossi, R. Cristel, P. L. Bonora, Corrosion and wear behaviour of HVOF cermet coatings used to replace hard chromium, *Electrochim. Acta*, 49(2004), 2803–2812.
  7. J. Wang, L. Zhang, B. Sun, and Y. Zhou, Study of the Cr<sub>3</sub>C<sub>2</sub>-NiCr Detonation Spray Coating, *Surf. Coat. Technol.*, 130(2000), 69–73.
  8. S. Matthews, Development of high carbide dissolution/low carbon loss Cr<sub>3</sub>C<sub>2</sub>-NiCr coatings by shrouded plasma spraying, *Surf. Coat. Technol.*, 258(2014), 886–900.
  9. H. Wang, H. Li, H. Zhu, F. Cheng, D. Wang, Z. Li, A comparative study of plasma sprayed TiB<sub>2</sub>-NiCr and Cr<sub>3</sub>C<sub>2</sub>-NiCr composite coatings, *Mater. Letters*, 153(2015), 110–113.
  10. L. Zhang, J. B. Hou, Study of microstructure and phase of plasma sprayed Cr<sub>3</sub>C<sub>2</sub>-NiCr coating before and after the sparking plasma sintering, *Physica Procedia*, 50(2013), 293–296.
  11. G. C. Ji, C. J. Li, Y. Y. Wang, W.I. Li, Erosion Performance of HVOF-Sprayed Cr<sub>3</sub>C<sub>2</sub>-NiCr Coatings, *J. Therm. Spray Technol.*, 16(2007), 557–565.
  12. G. Bolelli, L. M. Berger, T. Börner, H. Koivuluoto, V. Matikainen, L. Lusvardi, C. Lyphout, N. Markocsan, P. Nylén, P. Sassatelli, R. Trache, P. Vuoristo, Sliding and abrasive wear behaviour of HVOF- and HVAF-sprayed Cr<sub>3</sub>C<sub>2</sub>-NiCr hardmetal coatings, *Wear*, 358–359(2016), 32–50.
  13. Z. Marcano, J. Lesage, D. Chicot, G. Mesmacque, E. S. Puchi-Cabrera, M. H. Staia, Microstructure and adhesion of Cr<sub>3</sub>C<sub>2</sub>-NiCr vacuum plasma sprayed coatings, *Surf. Coat. Technol.*, 202(2008), 4406–4410.
  14. M. Hrabovsky, Water-stabilized plasma generators, *Pure Appl. Chem.*, 70(1998), 1157–1162.
  15. Standard test method for determination of slurry abrasivity (Miller number) and slurry abrasion response of materials (SAR number), ASTM: G 75 – 95, USA, 1995.
  16. P. Ctibor, K. Neufuss, F. Zahalka, B. Kolman, Plasma sprayed ceramic coatings without and with epoxy resin sealing treatment and their wear resistance, *Wear*, 262(2007), 1274–1280.
  17. P. Ctibor, K. Neufuss, P. Chraska, Microstructure and Abrasion Resistance of Plasma Sprayed Titania Coatings, *J. Therm. Spray Technol.*, 15 (2006), 689–694.
  18. H. Ageorges, P. Ctibor, Comparison of the structure and wear resistance of Al<sub>2</sub>O<sub>3</sub>-13 wt%TiO<sub>2</sub> coatings made by GSP and WSP plasma process with two different powders, *Surf. Coat. Technol.*, 202(2008), 4362–4368.
  19. Standard Test Method for Measuring Abrasion using the Dry Sand/Rubber Wheel Apparatus, ASTM: G 65-00-1, USA, 2001.
  20. S. Matthews, L. M. Berger, Long-term compositional/microstructural development of Cr<sub>3</sub>C<sub>2</sub>-NiCr coatings at 500 °C, 700 °C and 900 °C, *Int. J. Refrac. Metals Hard Mater.*, 59(2016), 1–18.
  21. M. Kašparová, F. Zahálka, Š. Houdková, WC-Co and Cr<sub>3</sub>C<sub>2</sub>-NiCr Coatings in Low- and High-Stress Abrasive Conditions, *J. Therm. Spray Technol.*, 20(2011), 412–420.
  22. R. Batia, Development of Erosion-Corrosion Resistant HVOF Sprayed Cr<sub>3</sub>C<sub>2</sub>-NiCr Coatings for Boiler Tube Steels Operating at Elevated Temperatures, Ph.D. thesis, University College of Engineering, Punjabi University, Patiala, Punjab, India, 2013.
  23. L. Janka, J. Norpoth, R. Trache, L.-M. Berger, Influence of heat treatment on the abrasive wear resistance of a Cr<sub>3</sub>C<sub>2</sub>-NiCr coating deposited by an ethene-fuelled HVOF spray process, *Surf. Coat. Technol.*, 291(2016), 444–451.
  24. Z. Lina, X. Bin-shi, W. Hai-dou, W. Cheng-biao, Indentation size effect on the mechanical properties of supersonic plasma sprayed NiCr-Cr<sub>3</sub>C<sub>2</sub> coating, *Rare Metal Mater. Eng.*, 41(2012), 265–273.
  25. D. E. Wolfe, T. J. Eden, J. K. Potter, and A. P. Jaroh, Investigation and Characterization of Cr<sub>3</sub>C<sub>2</sub>-Based Wear-Resistant Coatings Applied by the Cold Spray Process, *J. Therm. Spray Technol.*, 15(2006), 400–412.
  26. H. Sarjas, P. Kulu, K. Juhani, M. Viljus, V. Matikainen, P. Vuoristo, Wear resistance of HVOF sprayed coatings from mechanically activated thermally synthesized Cr<sub>3</sub>C<sub>2</sub>-Ni spray powder, *Proc. Estonian Ac. Sci.*, 65(2016), 101–106.
  27. S. Singh Chatha, H. S. Sidhu, B. S. Sidhu, Characterisation and Corrosion-Erosion Behaviour of Carbide based Thermal Spray Coatings, *J. Minerals Mater. Charac. Eng.*, 11(2012), 569–586.

28. M. Antonov, I. Hussainova, Thermophysical properties and thermal shock resistance of chromium carbide based cermets, *Proc. Estonian Ac. Sci.*, 12(2006), 358–367.

How to cite this article:

P. Ctibor, M. Prantnerová, Plasma spraying and characterization of chromium carbide–nickel chromium coatings, *Prog. Color Colorants Coat.*, 9 (2016) 281-290.

